Solar Energy Materials & Solar Cells 140 (2015) 174–179

Contents lists available at ScienceDirect

Solar Energy Materials & Solar Cells

journal homepage: www.elsevier.com/locate/solmat

# Hybrid $TiO_2$–multiwall carbon nanotube (MWCNTs) photoanodes for efficient dye sensitized solar cells (DSSCs)

Umer Mehmood [a], Ibnelwaleed A. Hussein [a,*], Khalil Harrabi [b], M.B. Mekki [b], Shakeel Ahmed [c], Nouar Tabet [d]

[a] Department of Chemical Engineering, King Fahd University of Petroleum & Minerals (KFUPM),P.O. Box 5050, Dhahran 31261, Kingdom of Saudi Arabia
[b] Department of Physics, KFUPM, P.O. Box 5050, Dhahran 31261, Kingdom of Saudi Arabia
[c] Center for Refining & Petrochemicals, KFUPM, P.O. Box 5050, Dhahran 31261, Kingdom of Saudi Arabia
[d] Qatar Environment and Energy Research Institute, Qatar Foundation, Qatar

ARTICLE INFO

*Article history:*
Received 13 January 2015
Received in revised form
1 April 2015
Accepted 3 April 2015
Available online 28 April 2015

*Keywords:*
Hybrid photoanodes
DSSC
MWCNT
Density functional theory

ABSTRACT

Dye sensitized solar cells (DSSCs) based on $TiO_2$/MWCNTs composite with varying concentrations of CNTs (0, 0.03. 0.06, 0.09, 0.15, and 0.21 wt%), fabricated using N3 dye as a sensitizer. Transmission electron microscopy was used to confirm the dispersion of carbon nanotubes in $TiO_2$. UV–visible absorption spectroscopy, photocurrent–voltage characteristics, and electrochemical impedance spectroscopic measurements were conducted to characterize the DSSCs. The results show that the photo conversion efficiency is highly dependent on the concentration of CNTs in the photoanode. A solar cell based on a photoanode containing 0.03 wt% MWCNTs has a power conversion efficiency which is about 30% greater than that of the unmodified photoanode. A quantum modeling technique based on the density functional theory was used to investigate the thermodynamic aspects of the charge transport processes in DSSCs. Simulation results support the experimental data.



## 1. Introduction

The world energy demand is continually increasing and the world power consumption, which is 13 terawatts (TW) currently, is expected to reach about 28 TW by 2050 [1]. Fossil fuels, which are depleting rapidly, meet 80% of the energy requirement of the world [2]. Owing to the growing energy demand, exhaustion of oil resources, and global warming issues, there is a need for clean and renewable energy technologies. Photovoltaic technology is regarded as the most efficient among all the sustainable energy technologies such as tidal power, solar thermal, hydropower, and biomass [3]. Solar radiation reaching the earth is approximately $3 \times 10^{24}$ J per year, which is ten times the current energy demand [4]. Thus, the conversion of photo energy into electrical energy is generally considered the best way to resolve the impending energy crisis.

Owing to their convenient production and low cost, when compared to inorganic solar cells, DSSCs have received global attention in the past 15 years. CNTs have also found many applications due to their excellent morphological and electrical properties. Coincidentally, the discovery of DSSCs and CNTs were published in *Nature* in 1991, with Grätzel reporting the development of dye sensitized solar cell [5] and Iijima reporting the discovery of CNTs [6].

The dye, which is the major component of the DSSCs, absorbs sunlight and produces excitons. It is chemically bonded to the porous surface of a semiconductor. Currently, DSSCs based on ruthenium(II)-polypyridyl complexes have the best conversion efficiencies (PCE) of 13% under standard (Global Air Mass 1.5) illumination [7]. The high efficiencies of DSSCs based on ruthenium (II)-polypyridyl complexes can be attributed to their wide absorption range, good spectroscopic properties, and the photostability when incorporated into the final device. In addition, the carboxylate groups attached to the bipyridyl moiety lower the energy of the ligand $\pi*$ orbital. The general representation of carboxylic acid based sensitizers is [Ru $(dcbH_2)_2LL'$], where $dcbH_2$, and L and/or L′ represent anchoring ligands and ancillary ligands, respectively. An example of a high performance carboxylic acid based sensitizer is *cis*-[$Ru(dcbH_2)_2(NCS)_2$], which is also known as the N3 dye. Of the two crystalline forms of $TiO_2$ available, anatase and rutile, the former is preferred because the exciton mobility in rutile is less than in anatase due to the high packing density.

The efficiency of DSSCs is still low when compared with the silicon solar cells due to the recombination of injected electrons with the electrolyte (dark current) and the oxidized dye [8]. Therefore, in order to improve the PCE of DSSCs, it is necessary to reduce the charge recombination and accelerate the electron

* Corresponding author.
*E-mail address:* ihussein@kfupm.edu.sa (I.A. Hussein).

http://dx.doi.org/10.1016/j.solmat.2015.04.004
0927-0248/

transport [9]. As the CNTs show outstanding electrical conductivity [10–12], their incorporation in the photoanode may enhance the PCE of DSSCs by reducing the charge recombination.

The thermodynamic aspects of the charge transport processes in DSSCs were also investigated using DFT and time dependent DFT. It is an effective tool as compared to other high level quantum approaches because the computed orbitals are suitable for the typical MO-theoretical analyses and interpretations [13]. Many theoreticians have successfully applied this technique to calculate the electronic structure and properties of photosensitizers [13–19].

## 2. Computer simulations

All the DFT/TD-DFT calculations were executed using Amsterdam Density Functional (ADF) program (2013.01).

### 2.1. $TiO_2$ cluster model

BAND mode was used to simulate the anatase $TiO_2$ cluster. The tetragonal anatase crystal structure with a single layer (001) surface slab was selected and a $4 \times 1$ supercell was created from this slab. All atoms were mapped within the unit cell.

### 2.2. Simulation method

$TiO_2$ and carbon doped $TiO_2$ models were simulated by considering the generalized gradient approximation (GAD) at BYLP (Becke, Lee–Yang–Parr) level and triple-ζ polarization basis function. The ground state geometries of N3, TiO-N3, and N3–($TiO_2$–C) systems were optimized by applying a hybrid B3LYP level together with the triple-ζ polarization basis function. UV–vis spectra of N3 were simulated in methanol as the solvent. Here the conductor-like screening model (COSMO) was selected to take the solvent effects into account. While the excitation energies were examined using TD-DFT and the statistical average of orbital potentials (SAOP) model was used to inocrporate the solvation effects. Eighty singlet–singlet transitions, which are sufficient to fully define the entire absorption spectrum, were calculated. In all calculations, the relativistic effects were taken into account by the zero order regular approximation (ZORA) Hamiltonian in its scalar approximation.

Light harvesting efficiency (LHE) [20] and free energy of electron injection ($\Delta G^{inject}$) [18] can be calculated using the following equations:

$$LHE = 1–10^{-A} \quad (1)$$

"$A$" represents the absorption

$$\Delta G^{inject} = Eox^{dye*} - E_{CB} \quad (2)$$

$E_{CB}$ is the conduction band of the semiconductor and $Eox^{dye*}$ is the excited state potential of the dye, which can be expressed as [15]:

$$Eox^{dye*} = Eox^{dye} - \Delta E \quad (3)$$

Similarly $Eox^{dye}$ is the ground state potential of the dye and $\Delta E$ is the minimum energy of absorption associated with $\lambda_{max}$, while [16]

$$Eox^{dye} = - \text{HOMO} \quad (4)$$

## 3. Experimental

### 3.1. Preparation of hybrid photoanodes

First a suspension was prepared by sonicating 0.01 g of MWCNTs in 20 mL of ethanol for 4 h. Then a known quantity of the MWCNTs suspension was mixed with a known amount of the anatase $TiO_2$ paste (T/SP 14451, solaronix) to obtain a composite paste. Five composite samples of $TiO_2$–MWCNTs with the following concentration of MWCNTs were prepared; 0, 0.03. 0.06, 0.09, 0.15, and 0.21 wt%. Each $TiO_2$–MWCNTs composite paste was then tape casted on FTO glass substrate (2 mm,7 Ω/seq, solaronix) and annealed at 450 °C for 30 min. The thickness of each photoanode was determined using the cross sectional scanning electron microscopy

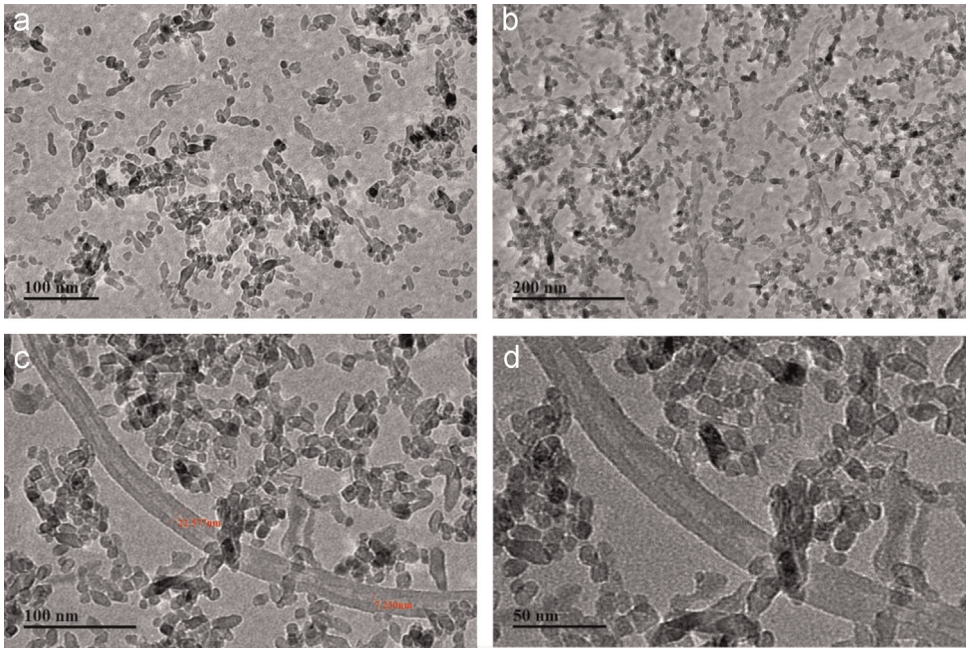


**Fig. 1.** Transmission electron microscopic images of (a) Pure $TiO_2$, (b) Dispersion of 0.15% MWCNTs in $TiO_2$, and Individual MWCNTs in the 0.15% dispersion of MWCNTs in $TiO_2$ at two magnifications, (c) 100 nm, and (d) 50 nm.

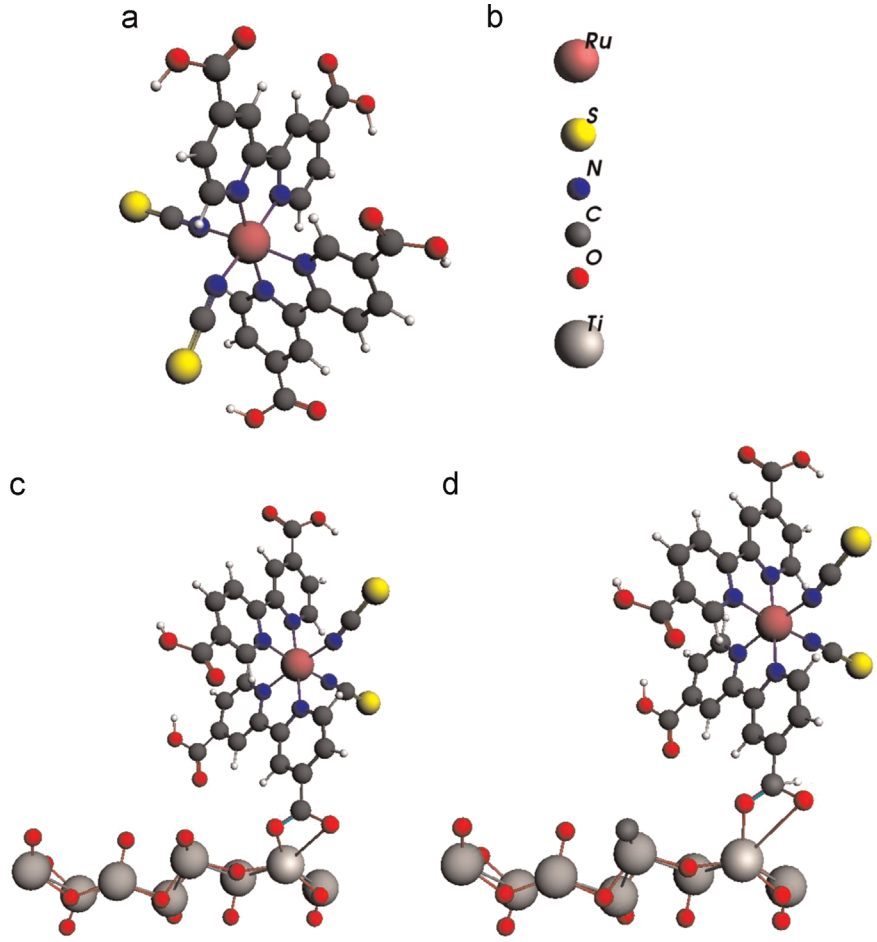


**Fig. 2.** Simulated structures of (a) N3, (b) legend of atoms, (c) $TiO_2$/N3 and (d) C–$TiO_2$/N3.

**Table 1a**
Simulated electronic properties of $TiO_2$ and carbon doped $TiO_2$.

| System | $E_{CB}$(eV) | $V_B$ (eV) | Band gap (eV) |
|---|---|---|---|
| $TiO_2$ | −4.1 | −7.2 | 3.1 |
| C–$TiO_2$ | −4.4 | −6.9 | 2.5 |

(SEM) images (JEOL, 6610LV). The average thickness of each film is 22 μm.

### 3.2. Fabrication and characterization of DSSCs

The hybrid electrodes were soaked in a 0.5 mM solution of N3 (Ruthenizer-535, solaronix) in methanol for 24 h. After sensitization, the samples were washed with alcohol to remove unanchored dye molecules. Then, DSSCs composed of a sensitized hybrid anode, a platinum deposited counter electrode (Plasticol T, solaronix), a 60-μm sealing spacer (Meltonix 1170, solaronix), and the electrolyte containing the $I^-/I_3^-$ redox couple (50 mM) in methoxypropionitrile (Iodolyte Z-50, solaronix) were fabricated.

UV–vis spectra of both Nin methanol and adsorbed on $TiO_2$ films on glass substrates were recorded with an Ocean Optics ISS-UV/VIS spectrophotometer. A Keithley 2400 SourceMeter was used to measure the *I–V* characteristics of the DSSCs using the IV-5 solar simulator (Sr #83, PVmeasurement, Inc.) at AM1.5G (100 mW $cm^{-2}$). The silicon solar cell was used as a reference for calibration. Charcaterization with electrochemical impedance spectroscopy (EIS) was conducted under dark conditions employing a Bio-Logic SAS (VMP3, s/n:0373), using an AC signal of 10 mV in amplitude, in the frequency range between 1 Hz and 1 MHz.

## 4. Results and discussion

The dispersion of MWCNTs in $TiO_2$ was verified using transmission electron miscroscopy (TEM), of a $TiO_2$–MWCNT sample with 0.15% CNT. This concentration was used because it is difficult to obtain TEM images of dispersed MWCNTs in $TiO_2$ at lower concentrations. The interface connection between MWCNTs and $TiO_2$ can be clearly observed in dispersions where MWCNTs are randomly distributed in $TiO_2$ (Fig. 1(b)), indicating that $TiO_2$ nanoparticles were attached to the surface of the MWCNTs well. The diameter of the coated MWCNTs significantly increases, and consequently the inner core of MWCNTs is hardly visible (Fig. 1(c and d)).

The HOMOs, LUMOs and band gap energies of photosensitizers play an important role in providing the thermodynamic driving force for the electron injection to the conduction band of $TiO_2$. For efficient charge transfer, the LUMOs of the dyes must be more negative than the conduction band of the semiconductor, while the HOMO levels must be more positive than the redox potential of the electrolyte. The simulated structures of N3, $TiO_2$/N3, and C–$TiO_2$/N3 are shown in Fig. 2. The electronic properties of the simulated conduction band, valence band, and the band gap of $TiO_2$ and C–$TiO_2$ are shown in Table 1a, while the properties of HOMOs, LUMOs, and the band gap of the photosensitizer are shown in Table 1b, which are in good agreement with experimental values [21, 22]. The computed results show that the doping of $TiO_2$ with MWCNTs (one of the

allotropic form of carbon) significantly reduces the band gap of the $TiO_2$ cluster. This is because the $E_{CB}$ of CNTs (~0 eV vs. NHE) is lower than that of $TiO_2$ (−0.5 eV vs. NHE) [11], which shifts the apparent Fermi level ($E_F$) to more positive potentials, i.e., a downward shift as shown in Fig. 3(a). Moreover, the thermodynamic driving force for charge transfer ($\Delta G^{inject}$) is defined as the energy difference between the excited state of the photosensitizer and the conduction band edge of the metal oxide. The downward positive shift due to MWCNTs can generate a significant driving force to facilitate the charge transfer from the excited dye to the conduction band of the photoanode. The simulated $\Delta G^{inject}$ value for C–$TiO_2$/N3 is greater than that of $TiO_2$/N3, as indicated in Table 3(b).

The UV–vis absorption spectra of N3 in methanol and anchored to $TiO_2$ and $TiO_2$–MWCNTs are shown in Fig. 4(a). The two broad bands in the visible region at 547 and 419 nm of N3 are assigned to metal-to-ligand charge-transfer (MLCT). The bands in the UV region at 322 nm are assigned to intraligand (π–π*) charge-transfer transitions. However, the absorption bands shift to lower energy values when N3 is anchored to $TiO_2$ and $TiO_2$–MWCNTs. This is due to the carboxylate groups binding to the $TiO_2$ surface through $Ti^{4+}$ acts as a proton. The interaction between the carboxylate groups and the surface $Ti^{4+}$ ions can increase the delocalization of the π* orbital. The energy of the π* level will decrease by delocalization, which explains the red shift of the absorption spectra. But the $TiO_2$–MWCNTs based photoanode has a greater red shift as compared to pure $TiO_2$. This is most likely due to the CNTs exhibiting photosensitizing properties, which extends the photovoltaic properties into the visible region [23]. Similarly, the simulated absorption spectra of N3, TiO-N3, and N3–$TiO_2$–MWCNTs shown in Fig. 4b are in good agreement with the experimental spectra. Thus, the COSMO solvation model with SOAP function is appropriate for computing the absorption spectra of these systems.

The *I–V* curves of the DSSCs based on hybrid photoanodes are shown in Fig. 5, while the device parameters, i.e., $J_{sc}$, $V_{oc}$ and FF, $R_{sh}$ (shunt resistance) and $R_s$ (series resistance) are shown in Table 2. The DSSC with the highest photo conversion (0.85%) efficiency is achieved with a film of 0.03% MWCNTs–$TiO_2$, which represents approximately a 30% increase with respect to pure $TiO_2$ (0.65%). The incorporation of MWCNTs in the $TiO_2$ network significantly enhances the efficiency of a DSSC due to the increase of the surface area of the hybrid anode, resulting in a higher dye loading. Moreover, the MWCNTs also improve the injection efficiency of the electrons due to the increased positive potential (as described above). Simulation results also confirm these results.

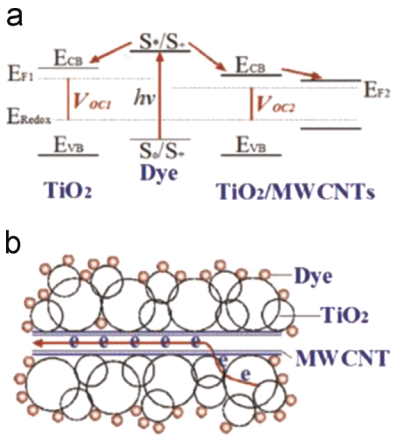


**Fig. 3.** The effect of the incorporation of MWCNTs in $TiO_2$ (a) shift of the energy levels and (b) enhancement of the electrical conductivity [11].

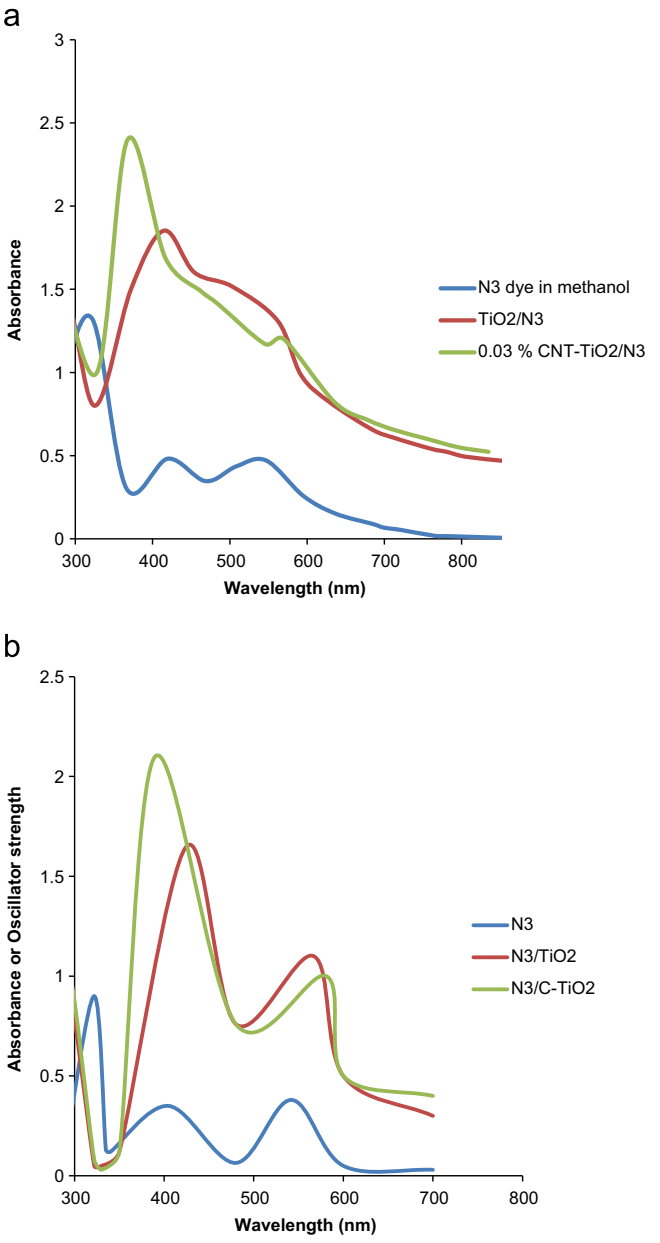


**Fig. 4.** (a) UV–vis spectra of N3, $TiO_2$, and CNTs–$TiO_2$/N3. (b) Simulated UV–vis spectra of N3, $TiO_2$/N3 and CNTs–$TiO_2$/N3.

**Table 1b**
Simulated electronic and optical properties of the photosensitizer.

| System | HOMO | LUMO | H–$L_{gap}$ | $\lambda_{max}$ | $\Delta E$ | $Eox^{dye}$ | $Eox^{dye*}$ | $\Delta G^{inject}$ | $A$ | *LHE |
|---|---|---|---|---|---|---|---|---|---|---|
| N3 | 5.63 | 3.67 | 1.96 | 542 | 2.29 | 5.63 | 3.34 | – | 0.9 | 87 |
| $TiO_2$/N3 | | | | 567 | 2.18 | | | 0.76 | 1.65 | 97 |
| C–TiO2/N3 | | | | 581 | 2.13 | | | 1.06 | 2.10 | 99 |

Units of HOMO, LUMO, H–$L_{gap}$, $\Delta E$, $Eox^{dye}$, $Eox^{dye*}$ and $\Delta G^{inject}$ are (eV). Unit of $\lambda_{max}$ is nm.
*LHE, corresponds to maximum *A*.

Table 1b shows that the absorption ($A$) or the oscillator strength of N3, $TiO_2$–N3, and N3–$TiO_2$–MWCNTs increase in the order of N–$TiO_2$–MWCNTs > N3–$TiO_2$ > N3. Thus, LHE will be in the order of N3–$TiO_2$–MWCNTs > N3–$TiO_2$ > N3. It demonstrates that higher the LHE the greater the photo current and hence the efficiency. However, the decrease of *Voc* with the increasing CNTs content can be attributed to the lowering of the potential band edge of $TiO_2$. As FF depends on both $R_s$ (should be low) and $R_{sh}$ (should be high), the FF values are low for these DSSCs (Table 2) which is supported by the measured high $R_s$ and low $R_{sh}$ values (Table 2). The low shunt resistance causes power losses in solar cells by providing an alternate pathway for the light-generated current, which lowers FF. $R_{sh}$ should be of the order of $10^3$ Ω for a highly efficient solar cell [24].The increase of the concentration of MWCNTs from the optimum level (0.03%) negatively affects the performance of DSSCs. This is attributed to the decrease in the film transparency owing to the increase of the MWCNTs content. Another cause of low efficiency at high MWCNT concentrations may be due to the formation of CNT agglomerates in the $TiO_2$ matrix, which act as trapping sites that obstruct the fast charge collection at the electrodes. Poor charge collection at the electrode coupled with the enhanced light loss due to direct absorption by CNTs, strongly reduces the efficiency of DSSCs at high CNTs content.

Electrochemical impedance spectroscopy (EIS) analysis is performed to further elucidate the photovoltaic properties. Fig. 6(a) shows the Nyquist plots of DSSCs based on $TiO_2$–N3 and 0.03% MWCNTS–$TiO_2$–N3. The interfacial charge transfer resistance ($R_2$) at the photoanode/electrolyte interface,obtained from the Nyquist plots, is related to the charge recombination rate, e.g., a smaller $R_2$ indicates a faster charge recombination. The $R_2$ value of a DSSC based on pure $TiO_2$ is smaller than that of 0.03% MWCNTs–$TiO_2$ DSSC as shown in Fig. 6(a), indicating that the charge recombination is greatly reduced owing to the incorporation of CNTs. However, the CNT concentrations greater than 0.03 wt% leads to smaller values of $R_2$ due to a shorter electron lifetime of the order of few tens of milliseconds [12]. Fig. 6 (b) shows the equivalent circuit of DSSCs, which describes the junction impedance. Table 3 shows all the of the equivalent electrical circuit, including the junction impedance, obtained from the EIS measurement system.

Regardless of the significant enhancement of PCE when 0.03 wt % CNTs is dispersed into the $TiO_2$ paste, the absolute value (0.85%) is exceptionally low as compared to the highest efficiency hitherto achieved (~12%) [5]. This is due to the photoanode film being too thick (22 μm), as the film thickness should be less than the electron diffusion length [25] for effective charge collection. The reported diffusion length of electrons in $TiO_2$ films, based on electron transport studies [26–28], is about 9–11 μm. A thick photoanode results

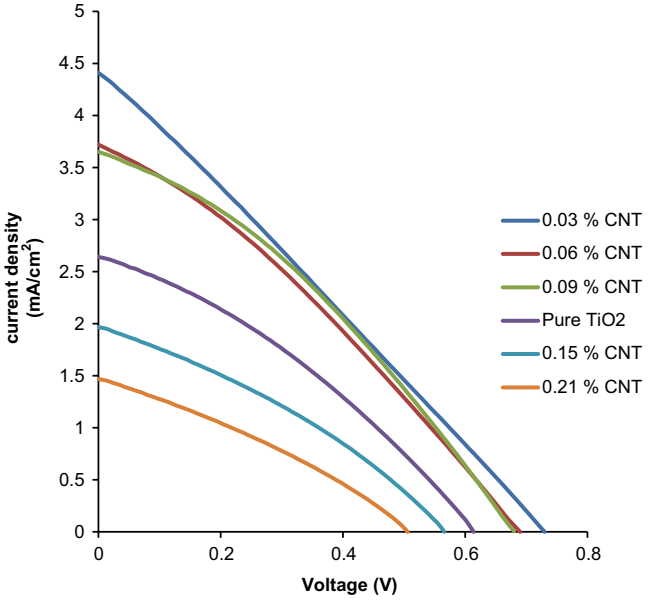


**Fig. 5.** Current–voltage curves of DSSCs fabricated using different concentrations of CNTs.

**Table 2**
Photovolatic properties of DSSCs based on hybrid anodes.

| No. | Anode structure | $j_{sc}$ (mA/cm$^2$) | $V_{oc}$ (mV) | FF(%) | η (%) | $R_{sh}$ (Ω) | $R_s$ (Ω) |
|---|---|---|---|---|---|---|---|
| 1 | $TiO_2$ | 2.651 | 617 | 33 | 0.64 | 116 | 42.37 |
| 2 | $TiO_2$+0.03% MWCNT | 4.415 | 730 | 27 | 0.85 | 52 | 66.66 |
| 3 | $TiO_2$+0.06% MWCNT | 3.715 | 686 | 31 | 0.78 | 98 | 47.62 |
| 4 | $TiO_2$+0.09% MWCNT | 3.652 | 679 | 34 | 0.83 | 118 | 51.21 |
| 5 | $TiO_2$+0.15% MWCNT | 1.974 | 569 | 32 | 0.37 | 121 | 80.21 |
| 6 | $TiO_2$+0.21% MWCNT | 1.475 | 506 | 31 | 0.23 | 112 | 95.23 |

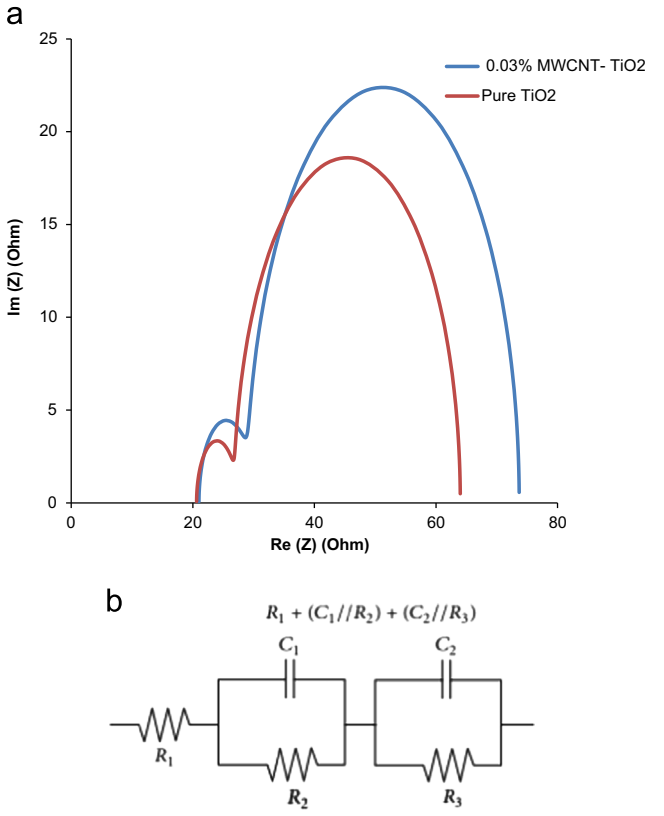


**Fig. 6.** (a) EIS investigation of the modified and unmodified DSSCs and (b) The equivalent circuit model of DSSC in which $R_1$: Serial resistance of FTO glass. $C_1\|R_2$: impedance at at $TiO_2$/dye/electrolyte interface, $C_2\|R_3$: impedance at Pt/electrolyte interface and:

**Table 3**
The resistances and capacitance values of DSSCs based on $TiO_2$ and $TiO_2$–MWCNTs.

| Photo anode | [a]$R_h$(Ω) | $R_1$(Ω) | $R_2$ (Ω) | $C_1$ (mF) | $C_2$ (mF) |
|---|---|---|---|---|---|
| $TiO_2$ | 20.62 | 6.235 | 37.15 | 20 | 0.57 |
| $TiO_2$–0.03% MWCNT | 21 | 8.023 | 44.65 | 23 | 0.45 |

[a] $R_h$ is the resistance for electron transport in the TCO substrate.

in a long electron diffusion distance to the FTO substrate (electrode), which increases the probability of recombination and thus degrades the efficiencies [29].

## 5. Conclusion

The dispersion of small amounts of MWCNTs in $TiO_2$ can significantly improve the photo conversion efficiency of DSSCs. Optimum concentration (0.03%) of CNTs does not affect the transparency of the $TiO_2$ layer, while significantly increasing the charge collection at the photoanode. The enhancement of electron lifetime, dye loading, and the reduction of the recombination phenomena leads to an increase in PCE of the DSSCs, with a maximum value of 0.85% (corresponding to the addition of 0.030 wt% MWCNTs). The DFT/TD-DFT simulation results also support the experimental data. This is a fast, cheap, and effective means of increasing the PCE of DSSCs.

## Acknowledgments

The authors would like to acknowledge the support provided by King Abdulaziz City for Science and Technology (KACST) through the Science & Technology Unit at King Fahd University of Petroleum & Minerals (KFUPM) for funding this work through Project #11-ENE1635-04 as part of the National Science, Technology and Innovation Plan. KFUPM (Project #11-ENE1635-04) is also acknowledged for supporting this research. The authors would like to acknowledge the Center of Research Excellence for Renewable Energy at KFUPM.

## References

[1] A. Hagfeldt, G. Boschloo, L. Sun, L. Kloo, H. Pettersson, Dye-sensitized solar cells, Chem. Rev. 110 (2010) 6595–6663. http://dx.doi.org/10.1021/cr900356p.
[2] B. Li, L. Wang, B. Kang, P. Wang, Y. Qiu, Review of recent progress in solid-state dye-sensitized solar cells, Sol. Energy Mater. Sol. Cells 90 (2006) 549–573. http://dx.doi.org/10.1016/j.solmat.2005.04.039.
[3] J. Gong, J. Liang, K. Sumathy, Review on dye-sensitized solar cells (DSSCs): fundamental concepts and novel materials, Renew. Sustain. Energy Rev. 16 (2012) 5848–5860. http://dx.doi.org/10.1016/j.rser.2012.04.044.
[4] K.R. Millington, Encyclopedia of Electrochemical Power Sources, Elsevier, Amsterdam, Netherlands (2009) http://dx.doi.org/10.1016/B978-044452745-5.00317-8.
[5] B. O'Regan, M. Grätzel, A low-cost, high-efficiency solar cell based on dye-sensitized colloidal $TiO_2$ films, Nature 353 (1991) 737–740. http://dx.doi.org/10.1038/353737a0.
[6] S. Iijima, Helical microtubules of graphitic carbon, Nature 354 (1991) 56–58. http://dx.doi.org/10.1038/354056a0.
[7] S. Mathew, A. Yella, P. Gao, R. Humphry-Baker, B.F.E. Curchod, N. Ashari-Astani, et al., Dye-sensitized solar cells with 13% efficiency achieved through the molecular engineering of porphyrin sensitizers, Nat. Chem. 6 (2014) 242–247. http://dx.doi.org/10.1038/nchem.1861.
[8] A. Kongkanand, R.M. Domínguez, P.V. Kamat, Single wall carbon nanotube scaffolds for photoelectrochemical solar cells. Capture and transport of photogenerated electrons, Nano Lett. 7 (2007) 676–680. http://dx.doi.org/10.1021/nl0627238.
[9] A. Hinsch, J.M. Kroon, R. Kern, I. Uhlendorf, J. Holzbock, A. Meyer, et al., Long-term stability of dye-sensitised solar cells, Prog. Photovolt. – Res. Appl. 9 (2001) 425–438. http://dx.doi.org/10.1002/pip.397.
[10] A. Kongkanand, P.V. Kamat, Electron storage in single wall carbon nanotubes. Fermi level equilibration in semiconductor-SWCNT suspensions, ACS Nano 1 (2007) 13–21. http://dx.doi.org/10.1021/nn700036f.
[11] P. Du, L. Song, J. Xiong, N. Li, L. Wang, Z. Xi, et al., Dye-sensitized solar cells based on anatase $TiO_2$/multi-walled carbon nanotubes composite nanofibers photoanode, Electrochim. Acta. 87 (2013) 651–656. http://dx.doi.org/10.1016/j.electacta.2012.09.096.
[12] K.T. Dembele, G.S. Selopal, C. Soldano, R. Nechache, J.C. Rimada, I. Concina, et al., Hybrid carbon nanotubes–$TiO_2$ photoanodes for high efficiency dye-sensitized solar cells, J. Phys. Chem. C 117 (2013) 14510–14517. http://dx.doi.org/10.1021/jp403553t.
[13] G. te Velde, F.M. Bickelhaupt, E.J. Baerends, C. Fonseca Guerra, S.J.A. van Gisbergen, J.G. Snijders, et al., Chemistry with ADF, J. Comput. Chem. 22 (2001) 931–967. http://dx.doi.org/10.1002/jcc.1056.
[14] J. Wang, H. Li, N.-N. Ma, L.-K. Yan, Z.-M. Su, Theoretical studies on organoimido-substituted hexamolybdates dyes for dye-sensitized solar cells (DSSC), Dyes Pigment. 99 (2013) 440–446. http://dx.doi.org/10.1016/j.dyepig.2013.05.027.
[15] W. Fan, D. Tan, W.-Q. Deng, Acene-modified triphenylamine dyes for dye-sensitized solar cells: a computational study, Chemphyschem 13 (2012) 2051–2060. http://dx.doi.org/10.1002/cphc.201200064.
[16] W. Sang-aroon, S. Saekow, V. Amornkitbamrung, Density functional theory study on the electronic structure of Monascus dyes as photosensitizer for dye-sensitized solar cells, J. Photochem. Photobiol. A – Chem. 236 (2012) 35–40. http://dx.doi.org/10.1016/j.jphotochem.2012.03.014.
[17] X. Zarate, E. Schott, T. Gomez, R. Arratia-Pérez, Theoretical study of sensitizer candidates for dye-sensitized solar cells: peripheral substituted dizinc pyrazinoporphyrazine–phthalocyanine complexes, J. Phys. Chem. A 117 (2013) 430–438. http://dx.doi.org/10.1021/jp3067316.
[18] J. Zhang, Y.-H. Kan, H.-B. Li, Y. Geng, Y. Wu, Z.-M. Su, How to design proper π-spacer order of the d-π-A dyes for DSSCs? A density functional response, Dyes Pigment. 95 (2012) 313–321. http://dx.doi.org/10.1016/j.dyepig.2012.05.020.
[19] D. Rocca, R. Gebauer, F. De Angelis, M.K. Nazeeruddin, S. Baroni, Time-dependent density functional theory study of squaraine dye-sensitized solar cells, Chem. Phys. Lett. 475 (2009) 49–53. http://dx.doi.org/10.1016/j.cplett.2009.05.019.
[20] F. Cervantes-Navarro, D. Glossman-Mitnik, Density functional theory study of indigo and its derivatives as photosensitizers for dye-sensitized solar cells, J. Photochem. Photobiol. A – Chem. 255 (2013) 24–26. http://dx.doi.org/10.1016/j.jphotochem.2013.01.011.
[21] R. Kavitha, L.G. Devi, Synergistic effect between carbon dopant in titania lattice and surface carbonaceous species for enhancing the visible light photocatalysis, J. Environ. Chem. Eng. 2 (2014) 857–867. http://dx.doi.org/10.1016/j.jece.2014.02.016.
[22] A. Anthonysamy, Y. Lee, B. Karunagaran, V. Ganapathy, S.-W. Rhee, S. Karthikeyan, et al., Molecular design and synthesis of ruthenium(ii) sensitizers for highly efficient dye-sensitized solar cells, J. Mater. Chem. 21 (2011) 12389. http://dx.doi.org/10.1039/c1jm11760b.
[23] K. Woan, G. Pyrgiotakis, W. Sigmund, Photocatalytic carbon-nanotube–$TiO_2$ composites, Adv. Mater. 21 (2009) 2233–2239. http://dx.doi.org/10.1002/adma.200802738.
[24] B. Tripathi, P. Yadav, M. Kumar, Charge transfer and recombination kinetics in dye-sensitized solar cell using static and dynamic electrical characterization techniques, Sol. Energy 108 (2014) 107–116. http://dx.doi.org/10.1016/j.solener.2014.06.037.
[25] T.G. Deepak, G.S. Anjusree, S. Thomas, T.A. Arun, S.V. Nair, A. Sreekumaran Nair, A review on materials for light scattering in dye-sensitized solar cells, RSC Adv. 4 (2014) 17615. http://dx.doi.org/10.1039/c4ra01308e.
[26] S. Nakade, M. Matsuda, S. Kambe, Y. Saito, T. Kitamura, T. Sakata, et al., Dependence of $TiO_2$ nanoparticle preparation methods and annealing temperature on the efficiency of dye-sensitized solar cells, J. Phys. Chem. B 106 (2002) 10004–10010. http://dx.doi.org/10.1021/jp020051d.
[27] S. Nakade, Y. Saito, W. Kubo, T. Kitamura, Y. Wada, S. Yanagida, Influence of $TiO_2$ nanoparticle size on electron diffusion and recombination in dye-sensitized $TiO_2$ solar cells, J. Phys. Chem. B 107 (2003) 8607–8611. http://dx.doi.org/10.1021/jp034773w.
[28] S. Nakade, W. Kubo, Y. Saito, T. Kanzaki, T. Kitamura, Y. Wada, et al., Influence of measurement conditions on electron diffusion in nanoporous $TiO_2$ films: effects of bias light and dye adsorption, J. Phys. Chem. B 107 (2003) 14244–14248. http://dx.doi.org/10.1021/jp035483i.
[29] J.K. Tsai, W.D. Hsu, T.C. Wu, T.H. Meen, W.J. Chong, Effect of compressed $TiO_2$ nanoparticle thin film thickness on the performance of dye-sensitized solar cells, Nanoscale Res. Lett. 8 (2013) 459. http://dx.doi.org/10.1186/1556-276X-8-459.